Revealing the Low-Temperature Interplay of Electronic, Ionic, and Optical Effects in Perovskite Electroluminescent Devices

Melanie H. Bowler,[1] Conor A. Ryan,[1] Aditya Mishra,[2] Anton V. Malko,[1] and Jason D. Slinker[1,2,3]*

[1]Department of Physics, The University of Texas at Dallas, 800 West Campbell Road, Richardson, Texas 75080-3021, United States.

[2]Department of Materials Science and Engineering, The University of Texas at Dallas, 800 West Campbell Road, Richardson, Texas 75080-3021, United States.

[3]Department of Chemistry, The University of Texas at Dallas, 800 West Campbell Road, Richardson, Texas 75080-3021, United States.

KEYWORDS Halide perovskites, mixed conductors, light-emitting electrochemical cells, temperature dependence, $CsPbBr_3$, LED stability

ABSTRACT: Perovskites are emerging as excellent candidates for light-emitting devices, and perovskite light-electrochemical cells (PeLECs) excel for their superior in-class stability due to the selective redistribution of additive ions. Here, to understand the interplay of ionic, electronic,

and optical effects and to assess the low-temperature stability of $CsPbBr_3$ PeLEC devices, we measured the temperature-dependent current, electroluminescence, and photoluminescence and investigated phase changes by differential scanning calorimetry and scanning electron microscopy. The radiant flux and external quantum efficiency of the device initially increased in cooling to 260 K, then decreased to 240K, and sharply declined at 220 K and below. However, photoluminescence primarily increased with decreasing temperature, suggesting that loss of luminance was due to frustrated charge transport. This dynamic follows from the onset of two glass transitions of the electrolyte and one phase transition of the $CsPbBr_3$ perovskite. Suppression of the polyelectrolyte glass transitions and perovskite phase transition through materials optimization could greatly improve the low-temperature performance of the devices. These features demonstrate that the interplay between the ionic, electronic, and optical properties of the devices relies greatly on the choice and physical properties of the polyelectrolyte and underlying perovskite.

Introduction

Perovskites are emerging as excellent candidates for light-emitting devices, evidenced by their rapid rise in reported external quantum efficiency.[1-7] Likewise, contributing to their rise, perovskites exhibit high color tunability and narrow emission bandwidths for high color purity, which halide substitutions of the perovskite lattice can achieve.[8-11] Perovskites are solution-processable materials, maintaining compatibility with glass and plastic substrates for lightweight and conformable light-emitting devices.[12, 13]

One challenge to implementing perovskites as light-emitting devices has been ion migration within the material, leading to hysteresis, color drift, and device failure. Our strategy for

achieving stable perovskite light-emitting devices is to fabricate them as perovskite light-emitting electrochemical cells (PeLECs).[14-20] PeLECs leverage ion motion to form electrical double layers (EDLs) at the electrodes[21, 22] and possible doping effects,[14] leading to efficient and balanced charge injection, resulting in high-efficiency performance from a single layer device. To avoid the detrimental effects associated with ionic dissociation of the perovskite lattice, these devices leverage differentiated ion motion through the motion of additive ions in place of the perovskite ions.[15, 18, 19] A polymer electrolyte (such as poly(ethylene oxide), PEO) and a salt with small, highly mobile ions (such as $LiPF_6$) are cast as a blended film with the perovskite. Under applied bias, the electrolyte facilitates the redistribution of the additive ions while preserving the perovskite structure. Differential ion motion in these PeLECs is strongly supported by the long-lasting devices produced[15, 20] and the color stability exhibited by devices with mixed halide perovskites.[18, 19] Thus, these devices exhibit rich device physics while offering high performance among perovskite light-emitting devices.

Much remains to be understood concerning the interplay of ionic motion, electronic transport, and emission in PeLECs. Temperature studies have shown value in probing the underlying physics of light-emitting electrochemical cells (LECs) while also evaluating the practical robustness of their operation. Gao et al. and Inayeh et al. cooled a polymer LEC below the glass transition of PEO to freeze ion motion and induce diode-like and photovoltaic behavior.[23-25] Building on this concept in recent works, Wang and coworkers applied reverse biases to similar "frozen junction" polymer LECs, evoking reverse bias EL.[26, 27] This reverse bias EL occurred in the same region as the forward bias EL and was attributed to tunnel injected electron combining with intrinsic holes. Slinker et al. performed a simultaneous temperature study of the photoluminescence and electroluminescence (EL) of ruthenium tris-bipyridine ($[Ru(bpy)_3^{2+}]$)

single layer LECs.[28] The external quantum efficiency fully tracked the temperature dependence of the photoluminescence (PL), and the lowering of luminescence with temperature was modeled as thermal activation to a nonradiative *d-d* transition.[29] Irreversible, current-induced emission degradation was observed for temperatures greater than room temperature. Bowler et al. subsequently investigated the temperature-dependent EL of Ru and Ir LECs, finding the Ir complexes to have substantially greater temperature stability, with an onset of LEC emission loss raised to 67 °C.[30] The temperature-dependent PL of the Ir complex showed a complex behavior modeled as a five-state system. Compared to the Ru complex, the superior emission and stability of the Ir complex were found to be due to favorable relative emission rates rather than energetic splitting. Ràfols-Ribé et al. utilized infrared imaging to discern that a current density of 50 mA cm^{-2} could induce self-heating to 50 °C of a Super Yellow polymer LEC. [31] This self-heating could be avoided by utilizing a device architecture with high thermal conductance and minimal active area fill factor.[31] Ribé et al. recently demonstrated that while polymer OLEDs were relatively temperature independent from 20 °C and 80 °C, polymer LECs from the same materials were strongly temperature dependent due to the drift of the recombination zone.[32]

Perovskite temperature dependence studies have revealed a diversity of emissive behaviors based on the size and composition of the perovskite crystals. Diroll et al. investigated the PL properties of a range of $CsPbX_3$ nanocrystals, where X is a halide, from 80 to 550 K.[33] The integrated PL values of these perovskite nanocrystals were highest at 80 K and lowered with temperature, dropping dramatically in the range of 300-500 K depending on the choice of halide. $CsPbBr_3$ exhibited the highest PL temperature resilience, while chlorine-containing crystals were the least robust. Time-resolved PL measurements revealed PL lifetimes initially increased with temperature due to exciton fission to form free carriers and then decreased due to trapping.[33] Han

and others studied similar $CsPbX_3$ nanocrystals, including mixed halides, and observed that all exhibited decreasing PL quantum yield (PLQY) in heating from 100 K to 300 K.[34] Both emission peak energies and linewidths increased with temperature. From time-resolved PL dynamics, it was concluded that biexponential PL decay resulted from a band-edge excitonic state and trapping state emission.[34] Alternatively, Zhang et al. found that nanocrystal films of $CsPbBr_3$ exhibited a PLQY that decreased with temperature to 200 K and subsequently increased.[35] This loss and subsequent recovery were explained by trapping, followed by thermal liberation from trap states. In addition, Naghadeh and colleagues demonstrated hybrid perovskite nanocrystals that increased, decreased, and remained unchanged in PL lifetime and emission energy from 100 K to 300 K, depending on the size of the nanocrystal.[36] Such dynamics were attributed to the interplay of polar domain formation versus insufficient surface passivation. Strandell and Kambhampati discovered discontinuities in the emission energies of $CsPbBr_3$ nanocrystals as a function of temperature indicative of a phase change between orthorhombic and cubic phases.[37] Recently, Chmeliov and others studied PeLEDs based on methylammonium lead iodide ($MAPbI_3$) surrounded by supporting hole and electron transport layers.[38] Complex current and EL dynamics were mathematically modeled and attributed to ionic redistribution in the perovskite layer, particularly iodine interstitials, with an activation energy of 175 meV. Recently, Mao and others compared the low-temperature performance of precharged polymer LECs against PeLEC devices, finding prebiased PeLECs to electroluminesce even at −193 °C.[39]

Here, we measured the temperature-dependent current, EL, and PL to understand the interplay of ionic, electronic, and optical effects and assess the low-temperature stability of PeLEC devices. We also investigated morphological changes by differential scanning calorimetry. The competing factors contributing to complex temperature performance are discussed, and the suite

of experiments presented enables the decoupling of these processes to assign causal relationships for the performance observed. These experiments reveal key factors in the underlying physics, morphology, and practical application of perovskite light-emitting devices.

Results and Discussion

PeLECs were fabricated with the structure ITO/PEDOT:PSS/$CsPbBr_3$:PEO:$LiPF_6$/LiF/Al and tested in a cryogenic probe station under vacuum at various temperatures. In particular, the PEO served as the polyelectrolyte and $LiPF_6$ as a salt with mobile ions to facilitate differential ion motion in the device and functionality as a PeLEC. See the inset of Figure 1 for a device structure. Samples were prepared with six accessible devices per device slide, with a photodiode mounted over the top of the device to collect electroluminescence. Sample slides were cooled, and each of the six devices was operated at precisely one temperature: either 280K, 260K, 240K, 220K, 200K, or 280 K after temperature cycling to 200 K. This allowed these six temperature experiments to be performed from fresh devices on the same slide. Device slides were cooled at ~4K/min and thermally equilibrated at each temperature for 5 min before operation. Devices were cooled in an open-circuit state, and, once thermally equilibrated, a 4 V bias was applied to investigate the transient effects at each temperature. This experiment was repeated five times, with a good qualitative agreement between experimental runs. This approach ensured that all devices on the slide were subject to the same preparation conditions and that each device started from an open circuit ion distribution.

For PeLECs, this method probes the impact of temperature on ionic redistribution in addition to charge transport and light emission processes. The current and EL from a PeLEC operating at 280 K to 200 K are shown in Fig. 1a and 1b, respectively. The current consistently lowers as the device is cooled, but the EL does not follow this trend. The EL (measured as

photocurrent from a photodiode) initially increases from 280 K to 260 K, then decreases as the temperature is lowered to 200 K. The EL is particularly chaotic at 220 K and 200 K, with brief spikes in the EL similar to those reported for a single-crystal device.[40] To view the overall trends in EL, the Fig. 1b data was smoothed with a 20-point moving average and plotted in Figure 1c (see Supporting Information Figure S1). Like prior PeLEC works, the EL versus time curves are structured.[15, 18] The overall trend of a decreasing EL from 260 K to 200 K is evident, as mirrored by the maximum EL trend versus temperature shown in Fig. 1d. Notably, the EL for an unused device did not recover when the PeLEC was warmed back to 280 K after cooling to 200 K, indicating that irreversible degradation had occurred from temperature cycling apart from device operation. The origin of this overall drop in EL with temperature requires further clarification.

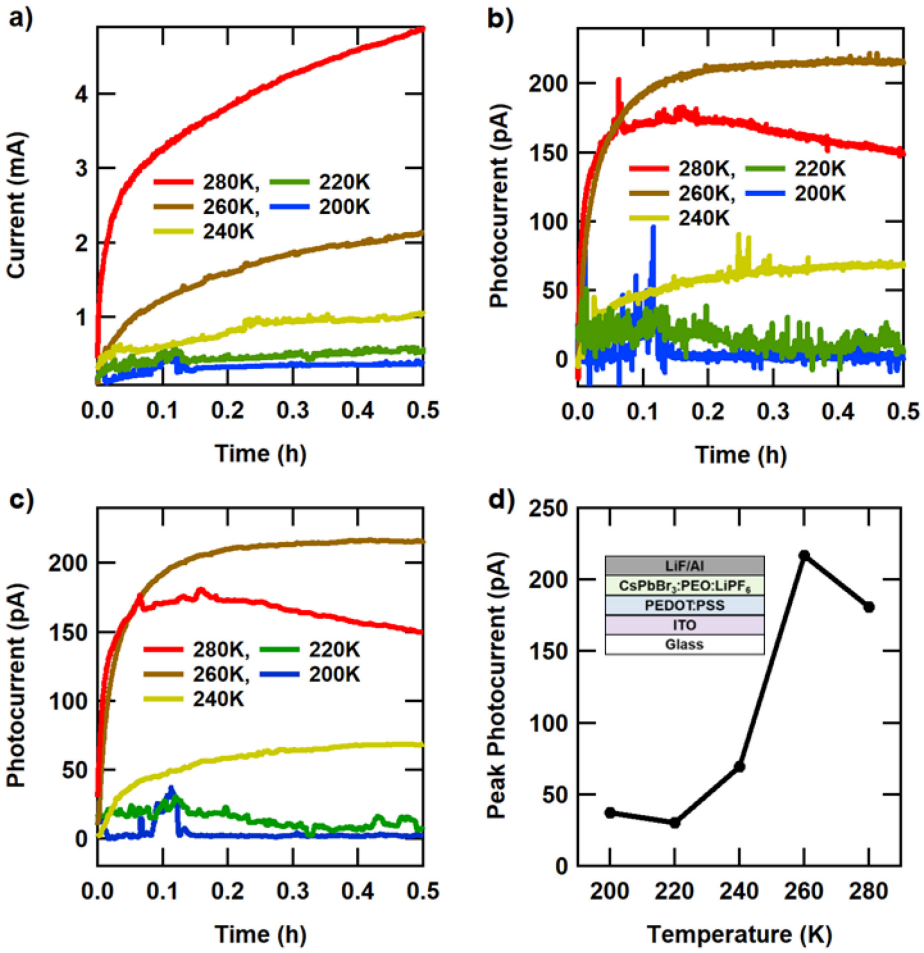

Figure 1. Temperature dependence of PeLEC device characteristics as the temperature is lowered from room temperature. (a) Current versus time for a $CsPbBr_3$ PeLEC under 4 V operation from 280 K to 200 K. (b) Raw photocurrent versus time arising from the radiant flux from a $CsPbBr_3$ PeLEC under 4 V operation from 280 K to 200 K. (c) Smoothed photocurrent data from Fig. 1b utilizing a 20-point moving average. (d) Peak photocurrent from Fig. 1c versus temperature from a $CsPbBr_3$ PeLEC under 4 V operation from 280 K to 200 K. (Inset) ITO/PEDOT:PSS/$CsPbBr_3$:PEO:$LiPF_6$/LiF/Al.

The trend of external quantum efficiency (EQE) with temperature follows a similar profile as the EL, as seen in Fig. 2a. Heuristically, we can break down EQE (η_{ext}) into three processes,

$$\eta_{ext} = b\Phi f = b\Phi \frac{1}{2n^2} \quad (1)$$

where b is the recombination efficiency—the fraction of charge carriers that form excitons, Φ is the fraction of excitons that decay radiatively, and f is the outcoupling factor, equal to $(2n^2)^{-1}$ for a flat thin-film device, where n is the refractive index of the glass.[41] As n has a very shallow temperature dependence,[42] the significant temperature dependence of the EQE relies on the carrier injection and transport properties controlling b, and Φ, which is approximated by the solid-state photoluminescence (PL) quantum yield of the film. Thus, the solid-state photoluminescence could partially elucidate PeLEC temperature dynamics.

Figure 2b-2d presents the PL spectra and estimated relative PL quantum yield (PLQY) of thin films of $CsPbBr_3$:PEO:$LiPF_6$ on glass when measured at temperatures between 280 K and 180 K. The PL spectra of Figure 2c relate the effect of cooling the film from 280 K to 180 K. The thin film PL generally increases with decreasing temperature, reaching a peak value at 180 K that is 74% higher than the peak at 280 K. In Figure 2d, the PL lowers as the film is heated, ultimately returning to a spectrum at 280 K lower in intensity than the original spectrum. These spectra were converted to an energy scale and integrated to estimate the relative PLQY as a function of temperature (Figure 2b). On cooling to 180 K, the PLQY exhibits a shallow increase, ~14% higher than the initial value. On heating back to 280 K, the PLQY lowers, closely tracking the cooling PLQY values until ~260 K, where the PLQY trends lower than the cooling values. Notably, the overall temperature trend of PLQY significantly differs from that of the PeLEC EQE (Figure 2a),

indicating that a factor impacting the carrier dynamics is likely contributing to the low-temperature dynamics.

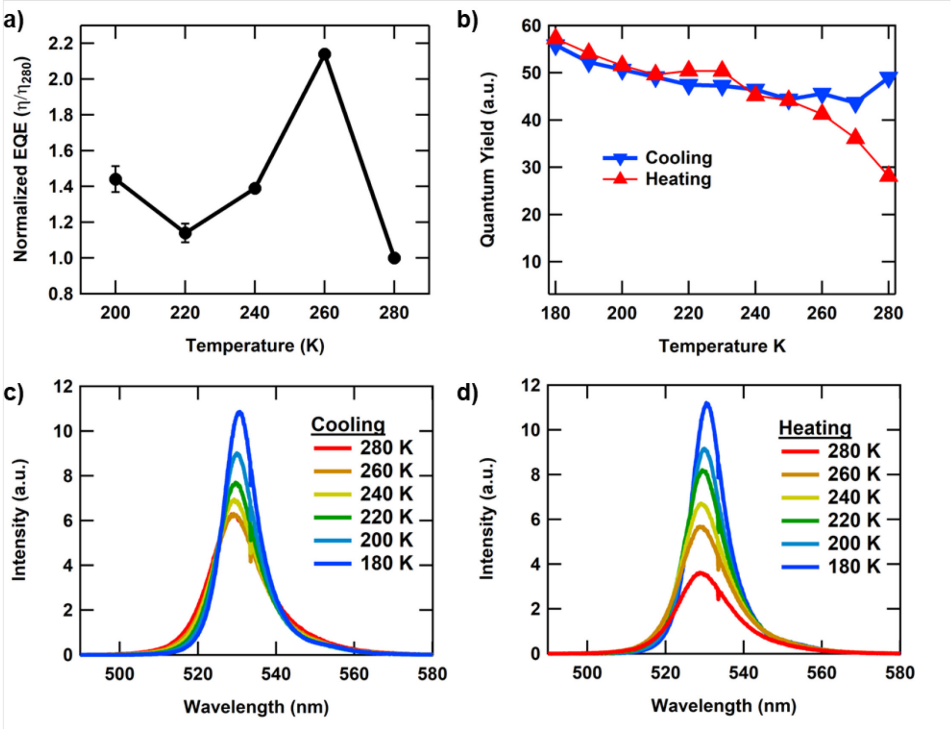

Figure 2. Temperature dependence of efficiency metrics and photoluminescence from 280 K to 180 K. (a) Normalized external quantum efficiency at maximum EL versus temperature from a $CsPbBr_3$ PeLEC under 4 V operation from 280 K to 200 K. Error bars were derived from the efficiency variance near each peak. (b) Estimated quantum yield versus temperature of thin films of $CsPbBr_3$:PEO:0.5% $LiPF_6$ cycled from 280 K to 180 K and back. (c) Photoluminescence spectra (λ_{ex} = 400 nm) of thin films of $CsPbBr_3$:PEO:0.5% $LiPF_6$ when cooled from 280 K to 180 K. (d) Photoluminescence spectra (λ_{ex} = 400 nm) of thin films of $CsPbBr_3$:PEO:0.5% $LiPF_6$ when heated from 180 K to 280 K.

Carrier recombination efficiency is dictated by the relative rates of hole and electron injection and transport through the bulk of the material. Morphological changes induced by temperature would greatly affect the structure of the perovskite film, likely leading to diminished injection and

transport while increasing charge carrier trapping. Perovskites can undergo phase transitions depending on the particulars of their structure, while the PEO electrolyte exhibits glass transition temperatures in the range of temperatures probed.[43-45] Differential scanning calorimetry (DSC) measures the heat required to change the temperature of a sample and is sensitive to phase transitions. **Figure 3** shows the DSC curves for PEO and $CsPbBr_3$ and the first derivatives of the DSC curves. A small differential is seen near 243-246 K, and a large transition is centered around 210 K. These are glass transitions for PEO.[43-45] For $CsPbBr_3$, an onset of a phase transition is observed near 213 K that peaks near 197 K. The transition near 245 K likely contributes to the loss of EL and luminance observed from 260 K to 240 K, and the highly energetic glass transitions near 210 K are likely catastrophic for electroluminescence at 220 K and 200K. These PEO and $CsPbBr_3$ transitions likely have significant detrimental effects on charge transport. We have established that stability in PeLEC devices is strongly tied to preserving the perovskite crystal structure in the perovskite:PEO:$LiPF_6$ blend matrix.[15, 18] Glass transitions are likely to introduce additional grain boundaries, defect states, and enhanced disorder that lower electroluminescence efficiency. Figure S2 of the Supporting Information reveals that while the EL of the reheated device at 280 K is negligible, the current recovers to a level near the original 280 K curve, albeit more slowly. This current dynamic suggests that while ionic transport is less efficient after cycling, it is still likely to form electrical double layers (EDLs). However, the low EL recovery coupled with the PL restoration demonstrates that the current is monopolar—either electrons or holes have been lost due to a lack of injection or transport. This monopolar current strongly contrasts the case in polymer LECs, where devices can be cooled below the PEO glass transition and subsequently reheated to recover significant luminance.[23-27] This contrasted performance likely occurs due to the amorphous nature of the conducting polymers in polymer LECs versus the highly ordered

crystals of PeLECs. Nonetheless, electrolyte temperature dependence can be dramatically changed by choice of materials,[46] so there is a strategic pathway forward if improved low-temperature stability is desired.

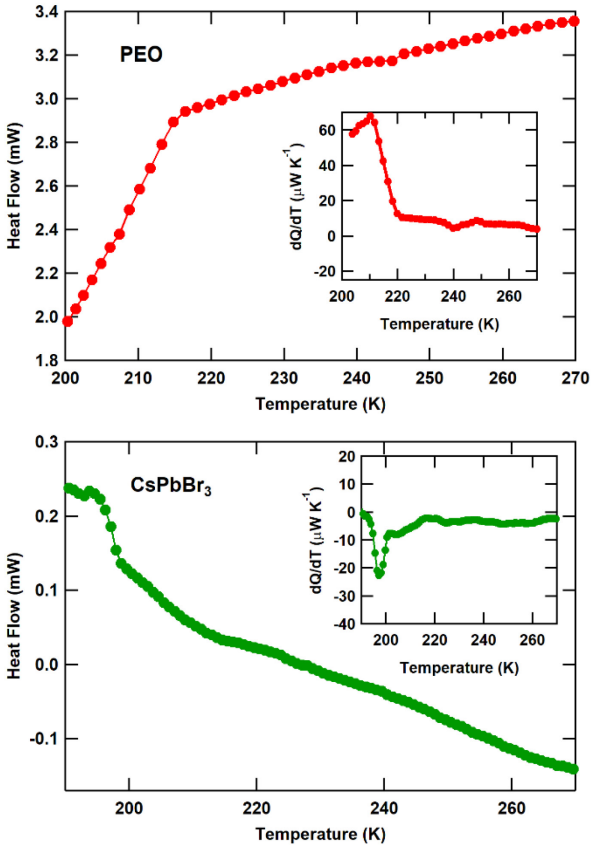

Figure 3. Differential scanning calorimetry (DSC) of PEO and $CsPbBr_3$. Heat flow versus temperature for PEO or $CsPbBr_3$. (Inset) The first derivative of heat flow versus temperature for PEO or $CsPbBr_3$ (averaged over five points for smoothing).

The lack of recovery of the EL and EQE upon reheating suggests that the disorder induced by these phase changes selectively impacts carrier dynamics. To verify this assertion, we performed scanning electron microscopy (SEM) imaging of $CsPbBr_3$:PEO:$LiPF_6$ films that were temperature cycled to 200 K under vacuum and compared to a control sample that was held at room temperature (Fig. 4). Comparison of the SEM images of Figure 4a and 4b show an overall similar thin-film

structure, but close inspection reveals a greater prevalence of grain boundaries in the thin film cycled to low temperature. These images were analyzed, and a histogram of the grain sizes for each image is shown in Fig. 4c and 4d. The extracted distributions shift to smaller grains for the low-temperature sample. Overall, the low temperature-cycled sample had an average grain size of 131 nm with a standard error of 7 nm, whereas the control sample was 147 ± 7 nm (t-test p-value = 0.08). Thus, the smaller grains and accompanying greater prevalence of grain boundaries of the low-temperature sample provide some rationale for the change in carrier dynamics.

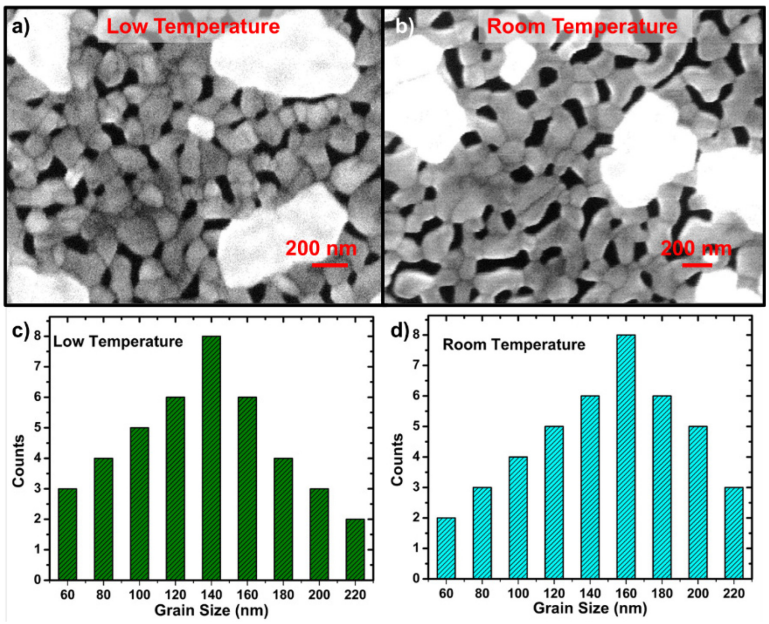

Figure 4. SEM of thin films of $CsPbBr_3$:PEO:$LiPF_6$ subject to various temperature processing. (a) SEM imaging of a $CsPbBr_3$:PEO:$LiPF_6$ thin-film temperature cycled to 200 K and back to room temperature. (b) SEM imaging of a control $CsPbBr_3$:PEO:$LiPF_6$ thin-film maintained at room temperature. (c) Histogram of the grain sizes obtained from the Figure 4a image for the low temperature cycled film. (d) Histogram of the grain sizes obtained from the Figure 4b image for the room temperature control film.

Finally, we also studied the performance of the PeLEC under steady state (always on) conditions under a 3V bias as it was cooled from room temperature under vacuum. We found that slow cooling on the order of 2 K/min to 200 K induced a 51% decrease in the luminance and a partial recovery to 64% of the initial value when reheated. Alternatively, rapid cryogenic cooling of ~20 K/min to 200 K induced a dramatic and irreversible drop to near zero luminance. The slow cooling likely allowed Joule heating to maintain a significantly higher local temperature of the PeLEC,[31] whereas the more rapid cooling likely overcame this effect and induced the rapid luminance loss from the phase transitions mentioned above.

Conclusions

This work demonstrates three regions of performance for PeLEC devices. Initially, lowering temperatures increases luminance due to improved carrier balance. In the second regime, below the first glass transition for PEO (~245 K), ion transport is frustrated, resulting in lowered current and luminance, but the PeLEC still functions with an efficiency near room temperature. In the third regime at 220 K and below, near the second glass transition for PEO and a phase transition for $CsPbBr_3$, ionic transport is greatly frustrated, leading to inefficient EDL formation and sporadic luminance. Luminance and efficiency do not recover on heating to room temperature, but the current does, indicating charge injection is monopolar after temperature cycling, likely due to morphological changes. This temperature behavior demonstrates that the interplay between the ionic, electronic, and optical properties of the devices relies greatly on the choice and physical properties of the polyelectrolyte and the perovskite. Suppression of the polymer glass transitions and perovskite phase transition could greatly improve the low-temperature performance of the

devices. Other polyelectrolytes, polymer gels, solid ceramics, crown ethers, ionic liquids, and molten salts may also be considered to accomplish the desired effects of differential ion motion within perovskite thin films and devices.

Experimental

Materials. Lead (II) bromide ($PbBr_2$; 99.99% trace metal basis), cesium bromide (CsBr; 99.99%) and polyethylene oxide (PEO; M.W. > 5,000,000) were all purchased from Alfa Aesar. Lithium hexafluorophosphate ($LiPF_6$; 99.99%) and dimethyl sulfoxide (DMSO; anhydrous > 99.9%) were purchased from Sigma Aldrich.

Perovskite Solution Preparation. The $CsPbB_3$ precursor solution was prepared by dissolving $PbBr_2$:CsBr (1:1.5 molar ratio) in DMSO and keeping it overnight for dissolution. PEO was prepared in DMSO solution (10mg/ml). The dissolved $CsPbBr_3$ and PEO were mixed in a 100:80 weight ratio. $LiPF_6$ (4mg/ml in DMSO) was added to this solution to make a final $CsPbBr_3$:PEO:$LiPF_6$ precursor solution with a 0.5% weight ratio of $LiPF_6$.

Device Fabrication. PeLECs were prepared with a device architecture of ITO/PEDOT:PSS/$CsPbBr_3$:PEO:$LiPF_6$/LiF/Al. Prepatterned indium tin oxide (purchased from Thin Film Devices, Anaheim, CA) was cleaned in a sequence of non-ionic detergent wash, water bath sonication, and UV ozone treatment. Aqueous poly(3,4-ethylenedioxythiophene): polystyrene sulfonate (PEDOT:PSS) solutions (1.3−1.7%, Clevios AI 4083) were filtered through a 0.45 μm GHP filter and spin-cast to obtain a ∼20 nm thick film on the ITO-coated glass substrates. Subsequently, these films were annealed at 100 °C for 10 minutes in a dry N_2-filled glovebox. Next, the active layer precursor solution was spin-cast onto PEDOT:PSS at 1500 rpm, vacuum treated in the glovebox load lock for 90 seconds, and then thermally annealed at 70 °C for

five minutes. The active layer thicknesses were generally 125-130 nm. For the top electrode, samples were transferred to a vacuum chamber, and 10 Å of LiF (which lowers the electrode workfunction) and 800 Å of Al were deposited using a shadow mask that defined 12 devices per substrate with a 3 mm^2 device area.

Device Testing. Testing was performed in a Lake Shore Cryotronics TTPX cryogenic probe station equipped with a Lake Shore model 336 temperature controller and a liquid nitrogen dewar with adapters for interface with a standard liquid helium transfer line. To capture light emission, a Hamamatsu S12915-1010R photodiode was taped over the device on the aluminum side such that emission was captured from the light reflected from the sample stage. Electrical connections to the PeLEC and photodiode were made with Lake Shore ZN50R-CVT-25-W and ZN50R-03-BECU probe tips. PeLEC current and electroluminescence were recorded with two Keithley 2450 source meters and Keithley 2.0 Kickstart software.

Photoluminescence measurements. The perovskite thin films were spin-cast onto glass substrates using the solution preparation noted in the device fabrication section. Temperature-dependent photoluminescence was measured with a custom setup. In short, thin-film samples on a glass slide were placed in a custom vacuum cryostat chamber. Excitation was achieved with a laser excitation near 400 nm, and photoluminescence spectra were captured with a spectrometer. The temperature was varied with a digital temperature controller, and data was recorded with a custom LabView program. Spectra were numerically integrated against an energy scale to estimate relative quantum yield.

Differential Scanning Calorimetry. 15 mg of polyethylene oxide powder and ~10 mg of $CsPbBr_3$ were tested in a Q2000 V24.10 differential scanning calorimeter (TA Instruments, New Castle, Delaware). The sample was cooled with a 10 °C/min ramp rate.

Scanning Electron Microscopy (SEM). Secondary electron SEM images were taken with a Zeiss Supra-40 SEM using an in-lens detector at an accelerating voltage of 10kV.

ASSOCIATED CONTENT

Supporting Information. The supporting information is available free of charge at:

Fitting to EL data, EL upon reheating, PL peak position, and full-width half max (PDF)

AUTHOR INFORMATION

Corresponding Author

*slinker@utdallas.edu

Author Contributions

The manuscript was written through the contributions of all authors. All authors have approved the final version of the manuscript.

Funding Sources

National Science Foundation **ECCS 1906505**

National Science Foundation **DGE 1746053**

Office of Naval Research **N00014-20-1-2220**

Eugene McDermott Graduate Fellowship 201801

ACKNOWLEDGMENT

J.D.S. acknowledges support from the National Science Foundation (ECCS 1906505) and the Office of Naval Research (N00014-20-1-2220). M.H.B acknowledges support from a National Science Foundation Graduate Research Fellowship (DGE 1746053) and a Eugene McDermott Graduate Fellowship (201801).

ABBREVIATIONS

PeLEC, perovskite light-emitting electrochemical cell; LEC, light-emitting electrochemical cell; EDLs, electrical double layers; PEO, poly(ethylene oxide); EL, electroluminescence; PL, photoluminescence; EQE, external quantum efficiency

REFERENCES

1. Lin, K. B.; Xing, J.; Quan, L. N.; de Arquer, F. P. G.; Gong, X. W.; Lu, J. X.; Xie, L. Q.; Zhao, W. J.; Zhang, D.; Yan, C. Z.; Li, W. Q.; Liu, X. Y.; Lu, Y.; Kirman, J.; Sargent, E. H.; Xiong, Q. H.; Wei, Z. H. Perovskite light-emitting diodes with external quantum efficiency exceeding 20 per cent. *Nature* **2018**, 562, 245-248.
2. Quan, L. N.; Rand, B. P.; Friend, R. H.; Mhaisalkar, S. G.; Lee, T. W.; Sargent, E. H. Perovskites for Next-Generation Optical Sources. *Chem. Rev.* **2019**, 119, 7444-7477.
3. Cao, Y.; Wang, N.; Tian, H.; Guo, J.; Wei, Y.; Chen, H.; Miao, Y.; Zou, W.; Pan, K.; He, Y.; Cao, H.; Ke, Y.; Xu, M.; Wang, Y.; Yang, M.; Du, K.; Fu, Z.; Kong, D.; Dai, D.; Jin, Y.; Li, G.; Li, H.; Peng, Q.; Wang, J.; Huang, W. Perovskite light-emitting diodes based on spontaneously formed submicrometre-scale structures. *Nature* **2018**, 562, 249-253.
4. Zhao, B.; Lian, Y.; Cui, L.; Divitini, G.; Kusch, G.; Ruggeri, E.; Auras, F.; Li, W.; Yang, D.; Zhu, B.; Oliver, R. A.; MacManus-Driscoll, J. L.; Stranks, S. D.; Di, D.; Friend, R. H. Efficient light-emitting diodes from mixed-dimensional perovskites on a fluoride interface. *Nat. Electron.* **2020**, 3, 704-710.
5. Cho, H. C.; Jeong, S. H.; Park, M. H.; Kim, Y. H.; Wolf, C.; Lee, C. L.; Heo, J. H.; Sadhanala, A.; Myoung, N.; Yoo, S.; Im, S. H.; Friend, R. H.; Lee, T. W. Overcoming the

electroluminescence efficiency limitations of perovskite light-emitting diodes. *Science* **2015**, 350, 1222-1225.
6. Protesescu, L.; Yakunin, S.; Bodnarchuk, M. I.; Krieg, F.; Caputo, R.; Hendon, C. H.; Yang, R. X.; Walsh, A.; Kovalenko, M. V. Nanocrystals of Cesium Lead Halide Perovskites (CsPbX3, X = Cl, Br, and I): Novel Optoelectronic Materials Showing Bright Emission with Wide Color Gamut. *Nano Lett.* **2015**, 15, 3692-3696.
7. Yantara, N.; Bhaumik, S.; Yan, F.; Sabba, D.; Dewi, H. A.; Mathews, N.; Boix, P. P.; Demir, H. V.; Mhaisalkar, S. Inorganic Halide Perovskites for Efficient Light-Emitting Diodes. *J. Phys. Chem. Lett.* **2015**, 6, 4360-4364.
8. Li, X.; Wu, Y.; Zhang, S.; Cai, B.; Gu, Y.; Song, J.; Zeng, H. CsPbX3 Quantum Dots for Lighting and Displays: Room-Temperature Synthesis, Photoluminescence Superiorities, Underlying Origins and White Light-Emitting Diodes. *Adv. Funct. Mater.* **2016**, 26, 2435-2445.
9. Tong, Y.; Bladt, E.; Aygüler, M. F.; Manzi, A.; Milowska, K. Z.; Hintermayr, V. A.; Docampo, P.; Bals, S.; Urban, A. S.; Polavarapu, L.; Feldmann, J. Highly Luminescent Cesium Lead Halide Perovskite Nanocrystals with Tunable Composition and Thickness by Ultrasonication. *Angew. Chem.-Int. Ed.* **2016**, 55, 13887-13892.
10. Song, J.; Li, J.; Li, X.; Xu, L.; Dong, Y.; Zeng, H. Quantum Dot Light-Emitting Diodes Based on Inorganic Perovskite Cesium Lead Halides (CsPbX3). *Adv. Mater.* **2015**, 27, 7162-7167.
11. Swarnkar, A.; Chulliyil, R.; Ravi, V. K.; Irfanullah, M.; Chowdhury, A.; Nag, A. Colloidal CsPbBr3 Perovskite Nanocrystals: Luminescence beyond Traditional Quantum Dots. *Angew. Chem.-Int. Ed.* **2015**, 54, 15424-15428.
12. Jia, P.; Lu, M.; Sun, S.; Gao, Y.; Wang, R.; Zhao, X.; Sun, G.; Colvin, V. L.; Yu, W. W. Recent Advances in Flexible Perovskite Light-Emitting Diodes. *Adv. Mater. Interfaces* **2021**, 8, 2100441.
13. Chu, S.; Chen, W.; Fang, Z.; Xiao, X.; Liu, Y.; Chen, J.; Huang, J.; Xiao, Z. Large-area and efficient perovskite light-emitting diodes via low-temperature blade-coating. *Nat. Commun.* **2021**, 12, 147.
14. Alahbakhshi, M.; Mishra, A.; Haroldson, R.; Ishteev, A.; Moon, J.; Gu, Q.; Slinker, J. D.; Zakhidov, A. A. Bright and Effectual Perovskite Light-Emitting Electrochemical Cells Leveraging Ionic Additives. *ACS Energy Lett.* **2019**, 4, 2922-2928.
15. Mishra, A.; Alahbakhshi, M.; Haroldson, R.; Bastatas, L. D.; Gu, Q.; Zakhidov, A. A.; Slinker, J. D. Enhanced Operational Stability of Perovskite Light-Emitting Electrochemical Cells Leveraging Ionic Additives. *Adv. Opt. Mater.* **2020**, 8, 2000226.
16. Mishra, A.; DiLuzio, S.; Alahbakhshi, M.; Adams, A. C.; Bowler, M. H.; Moon, J.; Gu, Q.; Zakhidov, A. A.; Bernhard, S.; Slinker, J. D. Bright Single-Layer Perovskite Host–Ionic Guest Light-Emitting Electrochemical Cells. *Chem. Mat.* **2021**, 33, 1201–1212.
17. Gets, D.; Alahbakhshi, M.; Mishra, A.; Haroldson, R.; Papadimitratos, A.; Ishteev, A.; Saranin, D.; Anoshkin, S.; Pushkarev, A.; Danilovskiy, E.; Makarov, S.; Slinker, J. D.; Zakhidov, A. A. Reconfigurable Perovskite LEC: Effects of Ionic Additives and Dual Function Devices. *Adv. Opt. Mater.* **2021**, 9, 2001715.
18. Mishra, A.; Alahbakhshi, M.; Haroldson, R.; Gu, Q.; Zakhidov, A. A.; Slinker, J. D. Pure Blue Electroluminescence by Differentiated Ion Motion in a Single Layer Perovskite Device. *Adv. Funct. Mater.* **2021**, 31, 2102006.

19. Mishra, A.; Alahbakhshi, M.; Gu, Q.; Zakhidov, A. A.; Slinker, J. D. Leveraging a Stable Perovskite Composite to Satisfy Blue Electroluminescence Standards. *ACS Mater. Lett.* **2021**, 3, 1357-1362.
20. Mishra, A.; Bose, R.; Zheng, Y.; Xu, W.; McMullen, R.; Mehta, A. B.; Kim, M. J.; Hsu, J. W. P.; Malko, A. V.; Slinker, J. D. Stable and Bright Electroluminescent Devices utilizing Emissive 0D Perovskite Nanocrystals Incorporated in a 3D CsPbBr3 Matrix. *Adv. Mater.* n/a, 2203226.
21. deMello, J. C. Interfacial feedback dynamics in polymer light-emitting electrochemical cells. *Phys. Rev. B* **2002**, 66, 235210.
22. Slinker, J. D.; DeFranco, J. A.; Jaquith, M. J.; Silveira, W. R.; Zhong, Y. W.; Moran-Mirabal, J. M.; Craighead, H. G.; Abruna, H. D.; Marohn, J. A.; Malliaras, G. G. Direct measurement of the electric-field distribution in a light-emitting electrochemical cell. *Nat. Mater.* **2007**, 6, 894-899.
23. Gao, J.; Yu, G.; Heeger, A. J. Polymer light-emitting electrochemical cells with frozen p-i-n junction. *Appl. Phys. Lett.* **1997**, 71, 1293-1295.
24. Inayeh, A.; Dorin, B.; Gao, J. Scanning photocurrent and photoluminescence imaging of a frozen polymer p-n junction. *Appl. Phys. Lett.* **2012**, 101, 253305.
25. Gao, J.; Li, Y.; Yu, G.; Heeger, A. J. Polymer light-emitting electrochemical cells with frozen junctions. *J. Appl. Phys.* **1999**, 86, 4594-4599.
26. Wang, D.; Hu, S.; Gao, J. Temperature Hypersensitive Organic Electroluminescence in a Reverse Biased, Frozen Polymer P–I–N Junction. *Adv. Opt. Mater.* **2021**, 9, 2101033.
27. Wang, D. Z.; Desroche, E.; Gao, J. Decoding the Polymer p-n Junction: Controlled Dedoping and Reverse Bias Electroluminescence. *Adv. Mater. Interfaces* **2020**, 7.
28. Slinker, J. D.; Malliaras, G. G.; Flores-Torres, S.; Abruña, H. D.; Chunwachirasiri, W.; Winokur, M. J. Temperature dependence of tris(2,2′-bipyridine) ruthenium (II) device characteristics. *J. Appl. Phys.* **2004**, 95, 4381-4384.
29. Van Houten, J.; Watts, R. J. Photochemistry of tris(2,2'-bipyridyl)ruthenium(II) in aqueous solutions. *Inorg. Chem.* **1978**, 17, 3381-3385.
30. Bowler, M. H.; Guo, T.; Bastatas, L. D.; Moore, M. D.; Malko, A. V.; Slinker, J. D. Understanding the superior temperature stability of iridium light-emitting electrochemical cells. *Mater. Horizons* **2017**, 4, 657-664.
31. Ràfols-Ribé, J.; Robinson, N. D.; Larsen, C.; Tang, S.; Top, M.; Sandström, A.; Edman, L. Self-Heating in Light-Emitting Electrochemical Cells. *Adv. Funct. Mater.* **2020**, 30, 1908649.
32. Ràfols-Ribé, J.; Gracia-Espino, E.; Jenatsch, S.; Lundberg, P.; Sandström, A.; Tang, S.; Larsen, C.; Edman, L. Elucidating Deviating Temperature Behavior of Organic Light-Emitting Diodes and Light-Emitting Electrochemical Cells. *Adv. Opt. Mater.* **2021**, 9, 2001405.
33. Diroll, B. T.; Nedelcu, G.; Kovalenko, M. V.; Schaller, R. D. High-Temperature Photoluminescence of CsPbX3 (X = Cl, Br, I) Nanocrystals. *Adv. Funct. Mater.* **2017**, 27, 1606750.
34. Han, Q.; Wu, W.; Liu, W.; Yang, Q.; Yang, Y. Temperature-dependent photoluminescence of CsPbX3 nanocrystal films. *J. Lumin.* **2018**, 198, 350-356.
35. Zhang, X. Y.; Pang, G. T.; Xing, G. C.; Chen, R. Temperature dependent optical characteristics of all-inorganic CsPbBr3 nanocrystals film. *Mater. Today Phys.* **2020**, 15, 100259.

36. Naghadeh, S. B.; Sarang, S.; Brewer, A.; Allen, A. L.; Chiu, Y.-H.; Hsu, Y.-J.; Wu, J.-Y.; Ghosh, S.; Zhang, J. Z. Size and temperature dependence of photoluminescence of hybrid perovskite nanocrystals. *J. Chem. Phys.* **2019**, 151, 154705.
37. Strandell, D. P.; Kambhampati, P. The Temperature Dependence of the Photoluminescence of CsPbBr3 Nanocrystals Reveals Phase Transitions and Homogeneous Linewidths. *J. Phys. Chem. C* **2021**, 125, 27504-27508.
38. Chmeliov, J.; Elkhouly, K.; Gegevičius, R.; Jonušis, L.; Devižis, A.; Gelžinis, A.; Franckevičius, M.; Goldberg, I.; Hofkens, J.; Heremans, P.; Qiu, W.; Gulbinas, V. Ion Motion Determines Multiphase Performance Dynamics of Perovskite LEDs. *Adv. Opt. Mater.* **2021**, 9, 2101560.
39. Mao, P.; Shan, X.; Li, H.; Davis, M.; Pei, Q.; Yu, Z. Iontronic Electroluminescence Devices: Comparing Halide Perovskites and Conjugated Polymers. *ACS Appl. Electron. Mater.* **2022**, 4, 568-575.
40. Andricevic, P.; Mettan, X.; Kollar, M.; Nafradi, B.; Sienkiewicz, A.; Garma, T.; Rossi, L.; Forro, L.; Horvath, E. Light-Emitting Electrochemical Cells of Single Crystal Hybrid Halide Perovskite with Vertically Aligned Carbon Nanotubes Contacts. *ACS Photonics* **2019**, 6, 967-975.
41. Kim, J.-S.; Ho, P. K. H.; Greenham, N. C.; Friend, R. H. Electroluminescence emission pattern of organic light-emitting diodes: Implications for device efficiency calculations. *J. Appl. Phys.* **2000**, 88, 1073-1081.
42. Tan, C. Z.; Arndt, J. Temperature dependence of refractive index of glassy SiO2 in the infrared wavelength range. *J. Phys. Chem. Solids* **2000**, 61, 1315-1320.
43. Calahorra, E.; Cortazar, M.; Guzmán, G. M. Spherulitic crystallization in blends of poly(ethylene oxide) and poly(methyl methacrylate). *Polymer* **1982**, 23, 1322-1324.
44. Kalfoglou, N. K.; Sotiropoulou, D. D.; Margaritis, A. G. Thermal and morphology characterization of blends of poly(ethylene oxide) with poly(vinyl acetate). *Eur. Polym. J.* **1988**, 24, 389-394.
45. Han, C. D.; Chung, H. S.; Kim, J. K. Rheology and phase behaviour of blends of poly(ethylene oxide) with poly(vinyl acetate) and with poly(vinyl acetate-ran-ethylene). *Polymer* **1992**, 33, 546-553.
46. Yu, G.; Cao, Y.; Andersson, M.; Gao, J.; Heeger, A. J. Polymer light-emitting electrochemical cells with frozen p-i-n junction at room temperature. *Adv. Mater.* **1998**, 10, 385-388.

For Table of Contents Only